Mechanics of Advanced Materials and Structures
Publication details, including instructions for authors and subscription information:
http://www.tandfonline.com/loi/umcm20

An Investigation into the Thermoelastic Analysis of Circular and Annular Functionally Graded Material Plates

M. E. Golmakani [a] & M. Kadkhodayan [a]
[a] Department of Mechanical Engineering , Ferdowsi University of Mashhad , Mashhad , Iran
Accepted author version posted online: 05 Jul 2012.Published online: 16 Sep 2013.

To cite this article: M. E. Golmakani & M. Kadkhodayan (2014) An Investigation into the Thermoelastic Analysis of Circular and Annular Functionally Graded Material Plates, Mechanics of Advanced Materials and Structures, 21:1, 1-13, DOI: 10.1080/15376494.2012.677101

To link to this article: http://dx.doi.org/10.1080/15376494.2012.677101

Mechanics of Advanced Materials and Structures (2014) **21**, 1–13

ISSN: 1537-6494 print / 1537-6532 online
DOI: 10.1080/15376494.2012.677101

Taylor & Francis
Taylor & Francis Group

An Investigation into the Thermoelastic Analysis of Circular and Annular Functionally Graded Material Plates

M. E. GOLMAKANI and M. KADKHODAYAN

Department of Mechanical Engineering, Ferdowsi University of Mashhad, Mashhad, Iran

Received 3 August 2010; accepted 1 June 2011.

The axisymmetric bending and stretching of circular and annular functionally graded plates with variable thicknesses under combined thermal-mechanical loading and various boundary conditions are investigated. The mechanical and thermal properties of functionally graded material (FGM) are assumed to vary continuously throughout the thickness of a plate in accordance with a simple power law of volume fraction of constituent material. Based on the first-order shear deformation theory, the governing equilibrium equations are derived, and the dynamic relaxation (DR) method is employed to solve these equations. Additionally, the effects of the thickness variation, temperature gradient, material constant n, and boundary conditions are discussed.

Keywords: thermoelastic analysis, FGM, circular and annular plates, DR method

1. Introduction

To eliminate interface problems and mitigate thermal stress concentrations in conventional laminated composite materials, functionally graded materials (FGMs) were first designed and introduced by a group of Japanese scientists in 1984 as thermal barrier materials for aerospace structural applications and fusion reactors [1]. In general, FGMs are microscopically inhomogeneous composites that are typically made from a mixture of metals and ceramics. This mixture can be achieved by gradually varying the composition of the constituent materials (typically only in the direction of thickness). FGMs have received a significant amount of attention in engineering applications, especially in high temperature environments, such as nuclear reactors, space planes, and chemical plants, due to their ability to withstand a high temperature gradient while maintaining structural integrity. Therefore, it is important to account for combined thermal-mechanical loading for the accurate, reliable analysis and design of FGM plates.

Based on the first-order shear deformation theory (FSDT), Praveen and Reddy [2] investigated the static and dynamic responses of a functionally graded (FG) plate under mechanical and thermal loads by using a finite element method. Based on the FSDT, the dynamic thermo-elastic response of functionally graded cylinders and plates was considered by Reddy and Chin [3]. Ferreira et al. [4] analyzed static deformations of functionally graded plates by using the collocation method, the radial basis functions, and a higher-order shear deformation theory. Ootao and Tanigawa [5] conducted an approximate analysis of three-dimensional thermal stresses in an FG rectangular plate. Reddy and Cheng [6] investigated three-dimensional thermo-mechanical deformations of a functionally graded rectangular plate. In their study, distributions of the temperature, displacements, and stresses in the plate were calculated for different volume fractions of ceramic constituent. The pseudo-dynamic thermoelastic response of functionally graded ceramic-metal cylinders was studied by Praveen et al. [7]. Using a perturbation approach, Obata and Noda [8] investigated thermal stresses in an FG hollow sphere and an FG hollow circular cylinder.

Although, extensive studies have been performed with respect to the thermal bending of functionally graded rectangular plates, thermoelastic analyses of circular and annular FGM plates and disks have received less attention. Based on the classical nonlinear von Karman plate theory, Ma and Wang [9] investigated the axisymmetric large deflection bending of a functionally graded circular plate under mechanical, thermal, and combined thermal–mechanical loading; they used the shooting method to numerically solve the equations. Based on FSDT, Bayat et al. [10] studied the thermoelastic analysis of functionally graded rotating disks with uniform and variable thicknesses under various boundary conditions. Bakhshi et al. [11] studied the dynamic thermoelastic behavior of an annular disk based on classical theory; in that study, a suitable transfinite element method was used to provide results in the time domain. There are also a small number of closed-form solutions for the elastic analysis of plates with variable thicknesses. Ohga and Shigematsu [12] used a combination of boundary-element and transfer-matrix methods to solve variable thickness rectangular plates. That method provided

Address correspondence to Mehran Kadkhodayan, Department of Mechanical Engineering, Ferdowsi University of Mashhad, Vakil-abad Street, Mashhad 91775-1111, Iran. E-mail: kadkhoda@um.ac.ir

a solution for only a special case of variable thickness rectangular plates. Fertis and Mijatov [13] developed a convenient, general method for the analysis of variable thickness plates with various boundary conditions and loading by using equivalent flat plates. Zenkour [14] presented an exact solution for the bending of thin rectangular plates with uniform, linear, and quadratic thickness variations. Xu and Zhou [15] presented a three-dimensional elasticity solution for rectangular FGM plates with variable thicknesses. To the knowledge of the authors, there is no literature regarding the thermoelastic response of a circular and annular functionally graded plate with uniform and variable thicknesses, that is, based on the FSDT.

In this study, an axisymmetric bending and stretching analysis of a circular and annular functionally graded plate under mechanical and combined thermal–mechanical loadings was investigated. The material properties of constituent materials in the FGM plate, except for Poisson's ratio (which is constant), were assumed to be graded in the thickness direction according to a power law distribution of the material composition. The plate was subjected to uniform pressure loading under various boundary conditions (simply supported and clamped). Due to the remarkable use of plates with variable thicknesses in engineering structures, four thickness profiles (constant, concave, convex, and linear) were employed to consider the effect of plate thickness. The dynamic relaxation (DR) method and a finite difference discretization technique were employed to solve the plate field equations. Validation of the DR solutions was performed by comparing the results to the exact solution reported by Reddy et al. [16]. Numerical results are presented to show the parametric effect of the material properties, plate thickness profile, boundary conditions, mechanical loading; and temperature fields on the different response characteristics of the FGM plates.

2. Theoretical Formulation

2.1. *FGM Modeling*

A functionally graded circular (or annular) plate with a thickness, inner radius, and outer radius of h, r_i, and r_0, respectively, was considered, as shown in Figure 1. The FGM plate was subjected to the transverse loading q and the thermal loading $\Delta T = T(z)$. Axial symmetry in the geometry and loading was assumed, and cylindrical coordinates (r, θ, z) were used. An FGM is typically made from a mixture of ceramics and metal with a continuously varying volume fraction throughout the thickness of the plate. Some models in the literature express the variation in the mechanical and thermal properties in the FGMs. The most commonly used model is the power law distribution of the volume fraction. According to this model, the material property gradation throughout the thickness of the plate p can be expressed as [3, 9]:

$$P(z) = (P_m - P_c)V_m + P_c, \tag{1}$$

where the subscripts m and c denote the metallic and ceramic constituents, respectively. The volume fraction of the metal V_m and ceramic V_c corresponding to the power law are assumed as:

$$\begin{cases} V_m = \left(\dfrac{h - 2z}{2h}\right)^n, \\ V_c = 1 - V_m, \end{cases} \tag{2}$$

where z is the thickness coordinate ($-h/2 \le z \le h/2$) and n is a material constant. According to this distribution, the bottom surface ($z = -h/2$) of the functionally graded plate is pure metal, and the top surface ($z = h/2$) is pure ceramic. Then different volume fractions of metal can be obtained for different values of n. This study assumes Poisson's ratio v to be constant and the elastic modulus E, thermal conductivity K, and thermal coefficient of expansion α to vary according to the gradation relation in Eq. (1). By substituting Eq. (1)

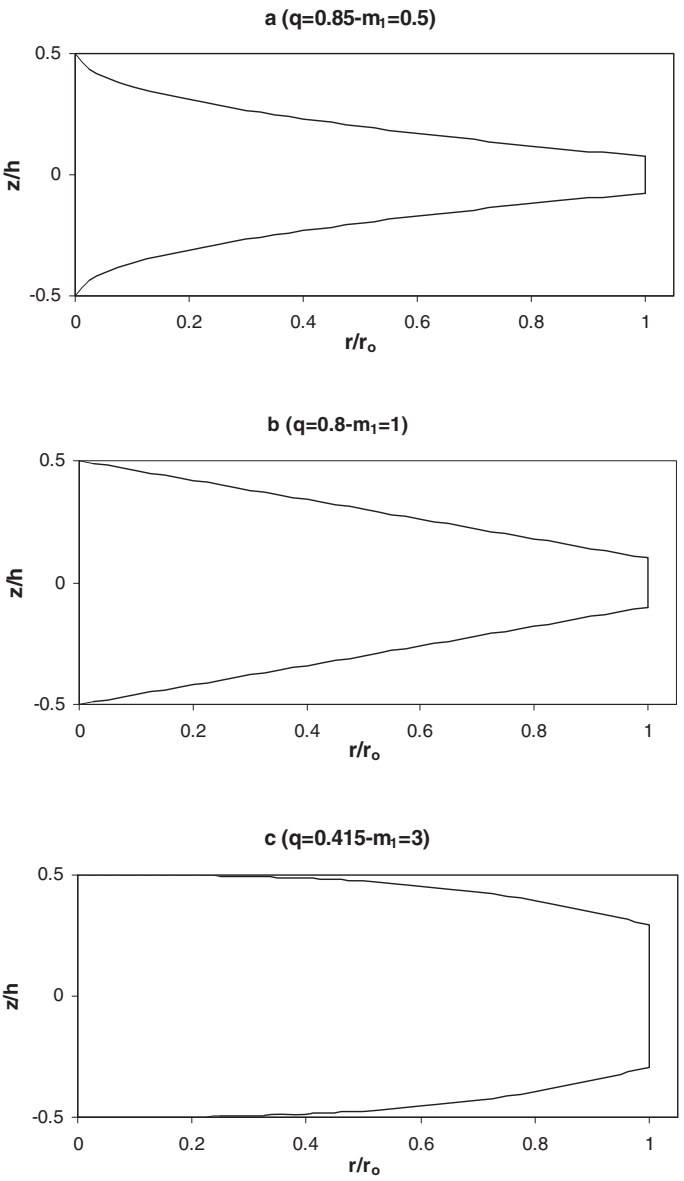

Fig. 1. Thickness profiles of the FGM plate: (a) concave, (b) linear, and (c) convex.

into Eq. (2), the material properties of the FGM plate are determined as:

$$\begin{cases} E(z) = (E_m - E_c)\left(\dfrac{h-2z}{2h}\right)^n + E_c, \\ \alpha(z) = (\alpha_m - \alpha_c)\left(\dfrac{h-2z}{2h}\right)^n + \alpha_c, \\ K(z) = (K_m - K_c)\left(\dfrac{h-2z}{2h}\right)^n + K_c, \\ v(z) = v, \end{cases} \tag{3}$$

where h changes along the radial direction if a plate with nonuniform thickness is considered. The thickness profile h of the plate is assumed to vary radially according to:

$$h(r) = h_o\left(1 - q\left(\frac{r}{r_o}\right)^{m_1}\right), \tag{4}$$

where q and m_1 are geometric parameters, such that $0 \le q < 1$, $m_1 > 0$, and h_o is the thickness at the center of the plate. A disk with uniform thickness can be obtained from Eq. (4) by setting $q = 0$, and a linearly decreasing thickness can be obtained for $q \neq 0$ and $m_1 = 1$. The profile is concave if $m_1 < 1$, or the profile is convex if $m_1 > 1$. Different forms of the thickness profiles for various values of q and m_1 are shown in Figure 1.

For thermal loading problems, it is assumed that the temperature variation is only along the thickness direction. The one-dimensional heat transfer equation for the z-direction is given by:

$$-\frac{d}{dz}\left(K(Z)\frac{dT(z)}{dz}\right) = 0, \tag{5}$$

with the boundary conditions $T(h/2) = T_c$ and $T(-h/2) = T_m$, and a stress-free state is assumed to exist at $T_0 = 0°\text{C}$. Here, the thermal conductivity coefficient $K(z)$ is in accordance with the power law relationship in Eq. (3). The temperature difference $T(z)$ can be obtained from Eq. (5) as [9]:

$$T(z) = T_m + (T_c - T_m)\int_{-h}^{z}\frac{dz}{K(z)}\Big/\int_{-h}^{h}\frac{dz}{K(z)}. \tag{6}$$

2.2. *Displacement Field and Strains*

The FSDT is a simple theory that accounts for nonzero transverse shear strain. In FSDT, the transverse shear strain is assumed to be constant with respect to the thickness coordinate. Shear correction factors are used to correct the inconsistency among the actual transverse shear-force distributions and the computed distributions using the kinematic relationships of the FSDT. This theory is based on the following displacement field [17]:

$$\begin{cases} u_r(r, z) = u_0(r) + z\psi(r), \\ u_z(r, z) = w(r), \end{cases} \tag{7}$$

where u_r and u_0 are displacements along the coordinate r. Also, u_z and w are displacements along the coordinate z. The term ψ denotes the rotation of a transverse normal at $z = 0$ of the deformed line that was straight in the un-deformed plate. By substituting Eq. (7) into the linear strain-displacement relationships of elasticity, the strain components are obtained as [18]:

$$\begin{cases} \varepsilon_r = \dfrac{\partial u_r}{\partial r} = \dfrac{du_0}{dr} + z\dfrac{d\psi}{dr}, \\ \varepsilon_\theta = \dfrac{u_r}{r} = \dfrac{u_0}{r} + z\dfrac{\psi}{r}, \\ \gamma_{rz} = \dfrac{\partial u_r}{\partial z} + \dfrac{\partial u_z}{\partial r} = \psi + \dfrac{dw}{dr}. \end{cases} \tag{8}$$

2.3. *Constitutive Relations*

According to Hooke's law, for a plate, the stress-strain relationships for the FGMs are given by:

$$\begin{cases} \sigma_r = \dfrac{E(z)}{(1-\nu^2)}[\varepsilon_r + \nu\varepsilon_\theta - (1+\nu)\alpha T(z)], \\ \sigma_\theta = \dfrac{E(z)}{(1-\nu^2)}[\varepsilon_\theta + \nu\varepsilon_r - (1+\nu)\alpha T(z)], \\ \sigma_{rz} = \dfrac{E(z)}{2(1+\nu)}\varepsilon_{rz}, \end{cases} \tag{9}$$

where ν is Poisson's ratio. The stress and moment resultants N_r, N_θ, M_r, M_θ, and Q_r are expressed as:

$$\begin{cases} (N_r, N_\theta, Q_r) = \displaystyle\int_{-h(r)/2}^{h(r)/2}(\sigma_r, \sigma_\theta, \sigma_{rz})dz, \\ (M_r, M_\theta) = \displaystyle\int_{-h(r)/2}^{h(r)/2}(\sigma_r, \sigma_\theta)z dz. \end{cases} \tag{10}$$

By substituting Eqs. (8) and (9) into Eq. (10), the constitutive relations are given as:

$$\begin{cases} N_r = A(r)\left(\dfrac{du}{dr} + \nu\dfrac{u}{r}\right) + B(r)\left(\dfrac{d\psi}{dr} + \nu\dfrac{\psi}{r}\right) - N_r^T, \\ N_\theta = A(r)\left(\dfrac{u}{r} + \nu\dfrac{du}{dr}\right) + B(r)\left(\dfrac{\psi}{r} + \nu\dfrac{d\psi}{dr}\right) - N_\theta^T, \\ M_r = B(r)\left(\dfrac{du}{dr} + \nu\dfrac{u}{r}\right) + C(r)\left(\dfrac{d\psi}{dr} + \nu\dfrac{\psi}{r}\right) - M_r^T, \\ M_\theta = B(r)\left(\dfrac{u}{r} + \nu\dfrac{du}{dr}\right) + C(r)\left(\dfrac{\psi}{r} + \nu\dfrac{d\psi}{dr}\right) - M_\theta^T, \\ Q_r = D(r)\left(\psi + \dfrac{dw}{dr}\right), \end{cases} \tag{11}$$

where $A(r)$, $B(r)$, $C(r)$, and $D(r)$ can be expressed as:

$$\begin{cases} (A(r),\, B(r),\, C(r)) = \displaystyle\int_{-h(r)/2}^{h(r)/2} \frac{E(z)}{1-\nu^2}(1,\, z,\, z^2)dz, \\ D(r) = \displaystyle\int_{-h(r)/2}^{h(r)/2} \frac{k_s E(z)}{2(1+\nu)}dz, \end{cases} \tag{12}$$

where $k_s = 5/6$ is the shear-correction factor. The membrane forces and bending moments in Eqs. (11) and (12) induced by thermal load can be calculated as:

$$\begin{cases} N_r^T = N_\theta^T = \displaystyle\int_{-h(r)/2}^{h(r)/2} \frac{E(z)}{1-\nu}\alpha(z)T(z)dz, \\ M_r^T = M_\theta^T = \displaystyle\int_{-h(r)/2}^{h(r)/2} \frac{E(z)}{1-\nu}\alpha(z)T(z)zdz. \end{cases} \tag{13}$$

2.4. *Equilibrium Equations*

For a circular plate, if U_1 is the total strain energy and V_1 is the total external work done on the body by the total specified external forces, then the total energy Π can be represented as $\Pi = U_1 - V_1$, where:

$$\begin{cases} U_1 = \displaystyle\int_V \sigma_{ij}\varepsilon_{ij}dV \\ \quad = \displaystyle\int_{r_i}^{r_o}\int_{-h(r)/2}^{h(r)/2} 2\pi(\sigma_r\varepsilon_r + \sigma_\theta\varepsilon_\theta + \sigma_{rz}\gamma_{rz})rdrdz, \\ V_1 = -\displaystyle\int_{r_i}^{r_o} 2\pi r q_z(r)u_z drdz, \end{cases} \tag{14}$$

where V represents the total volume of the plate and $q_z(r) = q$ is the vertical pressure applied to the surface of the plate. Using the principle of minimum total energy $\delta\Pi = 0$, the following equilibrium equations can be derived:

$$\begin{cases} \dfrac{dN_r}{dr} + \dfrac{1}{r}(N_r - N_\theta) = 0, \\ \dfrac{dM_r}{dr} + \dfrac{1}{r}(M_r - M_\theta) - Q_r = 0, \\ \dfrac{dQ_r}{dr} + \dfrac{Q}{r} + q = 0. \end{cases} \tag{15}$$

By substituting Eqs. (11), (12), and (13) into Eq. (15), the following three ordinary differential equations are derived for the displacement field:

$$\begin{cases} \dfrac{dA(r)}{dr}\left(\dfrac{du}{dr} + \dfrac{\nu u}{r}\right) + A(r)\left(\dfrac{d^2u}{dr^2} + \dfrac{1}{r}\dfrac{du}{dr} - \dfrac{u}{r^2}\right) \\ \quad + \dfrac{dB(r)}{dr}\left(\dfrac{d\psi}{dr} + \dfrac{\nu\psi}{r}\right) + B(r)\left(\dfrac{d^2\psi}{dr^2} + \dfrac{1}{r}\dfrac{d\psi}{dr} - \dfrac{\psi}{r^2}\right) \\ \quad - \dfrac{dN_r^T}{dr} = 0, \\ \dfrac{dB(r)}{dr}\left(\dfrac{du}{dr} + \dfrac{\nu u}{r}\right) + B(r)\left(\dfrac{d^2u}{dr^2} + \dfrac{\nu}{r}\dfrac{du}{dr} - \dfrac{\nu u}{r^2}\right) \\ \quad + \dfrac{dC(r)}{dr}\left(\dfrac{d\psi}{dr} + \dfrac{\nu\psi}{r}\right) + C(r)\left(\dfrac{d^2\psi}{dr^2} + \dfrac{\nu}{r}\dfrac{d\psi}{dr} - \dfrac{\nu\psi}{r^2}\right) \\ \quad + \dfrac{B(r)}{r}\left(\dfrac{du}{dr} + \dfrac{\nu u}{r} - \dfrac{u}{r} - \dfrac{\nu du}{dr}\right) + \dfrac{C(r)}{r}\left(\dfrac{d\psi}{dr} + \dfrac{\nu\psi}{r}\right. \\ \quad \left. - \dfrac{\psi}{r} - \nu\dfrac{d\psi}{dr}\right) - D(r)\left(\psi + \dfrac{dw}{dr}\right) - \dfrac{dM_r^T}{dr} = 0, \\ D(r)\left(\dfrac{d\psi}{dr} + \dfrac{d^2w}{dr^2} + \dfrac{\psi}{r} + \dfrac{1}{r}\dfrac{dw}{dr}\right) + \dfrac{dD(r)}{dr}\left(\psi + \dfrac{dw}{dr}\right) \\ \quad + q = 0. \end{cases} \tag{16}$$

2.5. *Boundary Conditions*

The following boundary conditions are used in this study:

(a) For a solid circular plate with a roller support at $r = r_o$:

$$\begin{cases} At \quad r = 0, \quad u = 0, \quad \psi = 0, \quad Q_r = 0, \\ At \quad r = r_o, \quad w = 0, \quad N_r = 0, \quad M_r = 0. \end{cases} \tag{17}$$

(b) For a solid circular plate with a hinged support at $r = r_o$:

$$\begin{cases} At \quad r = 0, \quad u = 0, \quad \psi = 0, \quad Q_r = 0, \\ At \quad r = r_o, \quad u = 0, \quad w = 0, \quad M_r = 0. \end{cases} \tag{18}$$

(c) For a solid circular plate with a clamped support at $r = r_o$:

$$\begin{cases} At \quad r = 0, \quad u = 0, \quad \psi = 0, \quad Q_r = 0, \\ At \quad r = r_o, \quad u = 0, \quad w = 0, \quad \psi = 0. \end{cases} \tag{19}$$

(d) For an annular plate with clamped inner and outer edges at $r = r_i$ and $r = r_o$:

$$\begin{cases} At \quad r = r_i, \quad u = 0, \quad w = 0, \quad \psi = 0, \\ At \quad r = r_o, \quad u = 0, \quad w = 0, \quad \psi = 0. \end{cases} \tag{20}$$

(e) For an annular plate with a clamped inner edge at $r = r_i$ and a simply supported outer edge at $r = r_o$:

$$\begin{cases} At \quad r = r_i, \quad u = 0, \quad w = 0, \quad \psi = 0, \\ At \quad r = r_o, \quad u = 0, \quad w = 0, \quad M_r = 0. \end{cases} \tag{21}$$

3. Numerical Solution Methodology

In this study, the dynamic relaxation (DR) method and a finite difference discretization technique were employed to solve the differential equations for the circular FGM plate under thermal and mechanical loading. Dynamic relaxation is an iterative method in which a static problem is converted into a dynamic problem by adding acceleration and damping terms; to obtain a steady-state solution. The explicit nature of the method makes it highly suitable for computers because all of the quantities can be treated as vectors, which results in an easily programmable method with low storage requirements. Day [19] first used this method to consider linear problems; during the next three decades, that technique was developed and used by other researchers to analyze linear and nonlinear responses of structural components, such as the bending, buckling, wrinkling, and stamping of plates [20–28]. It is convenient to first outline how the boundary value problem changes to an initial value format for the application of the DR procedure. Then some comments can be made regarding the numerical computations and the finite difference discretization.

3.1. *Dynamic Relaxation Method*

The DR method is essentially a pseudo-time-stepping initial-value technique. Therefore, to apply the DR method, it is necessary to convert the system of governing equations from boundary-value to initial-value format. The plate equations are transformed into DR format by adding the damping and inertia terms to the right-hand side of the equilibrium equations. Consequently, the equilibrium equations become:

$$\begin{cases} \dfrac{dN_r}{dr} + \dfrac{1}{r}(N_r - N_\theta) = m_u \dfrac{d^2u}{dt^2} + c_u \dfrac{du}{dt}, \\ \dfrac{dM_r}{dr} + \dfrac{1}{r}(M_r - M_\theta) - Q_r = m_\psi \dfrac{d^2\psi}{dt^2} + c_\psi \dfrac{d\psi}{dt}, \\ \dfrac{dQ_r}{dr} + \dfrac{Q}{r} = m_w \dfrac{d^2w}{dt^2} + c_w \dfrac{dw}{dt} - q, \end{cases} \tag{22}$$

where m_u, m_ψ, m_w and c_u, c_ψ, c_w are elements of the diagonal fictitious mass and the damping matrices M and C, respectively. In the DR method, the mass matrix and nodal damping factor should be defined to guarantee the stability and convergence of the iterative procedure. The most common method of determining $m_{ii}^l[l : u, \psi, w]$ at node i during the nth iteration is to use the Gershgörin theorem. According to this theorem, the following inequality must be satisfied to guarantee stability of the iterations:

$$m_{ii}^l \geq 0.25(\tau^n)^2 \sum_{j=1}^{N} \left| k_{ij}^l \right|, \tag{23}$$

where the superscript n represents the nth iteration step and τ is an increment of fictitious time. The element, k_{ij}, of the stiffness matrix, K, is calculated by:

$$K = \frac{\partial P}{\partial X}, \tag{24}$$

where $X = u,\ \psi,\ w$ is the approximate solution vector and P is the left-hand side of the equilibrium equations (Eq. (22)). Furthermore, based on the modified adaptive dynamic relaxation (maDR) method that was proposed by Zhang and Yu [28], the nodal damping factor c^n during the nth iteration is calculated by:

$$c^n = 2\left\{ \frac{(X^n)^t P(X^n)}{(X^n)^t M X^n} \right\}^{1/2}. \tag{25}$$

To complete the transformation process, the velocity and acceleration terms must be replaced with the following equivalent central finite-difference expressions [28]:

$$\dot{X}^{n-\frac{1}{2}} = (X^n - X^{n-1})/\tau^n, \tag{26}$$

$$\ddot{X}^n = (\dot{X}^{n+\frac{1}{2}} - \dot{X}^{n-\frac{1}{2}})/\tau^n. \tag{27}$$

By substituting Eqs. (26) and (27) into the right-hand side of Eq. (22), the equilibrium equations can be rearranged into an initial value format as follows:

$$\begin{cases} \dot{u}^{n+\frac{1}{2}} = \dfrac{2-\tau^n c^n}{2+\tau^n c^n}\dot{u}^{n-\frac{1}{2}} + \dfrac{2\tau^n}{2+\tau^n c^n} M^{-1} \\ \qquad\qquad \times \left(\dfrac{dN_r}{dr} + \dfrac{1}{r}(N_r - N_\theta) \right)^n, \\ \dot{\psi}^{n+\frac{1}{2}} = \dfrac{2-\tau^n c^n}{2+\tau^n c^n}\dot{\psi}^{n-\frac{1}{2}} + \dfrac{2\tau^n}{2+\tau^n c^n} M^{-1} \\ \qquad\qquad \times \left(\dfrac{dM_r}{dr} + \dfrac{1}{r}(M_r - M_\theta) - Q_r \right)^n, \\ \dot{w}^{n+\frac{1}{2}} = \dfrac{2-\tau^n c^n}{2+\tau^n c^n}\dot{w}^{n-\frac{1}{2}} + \dfrac{2\tau^n}{2+\tau^n c^n} M^{-1} \left(\dfrac{dQ_r}{dr} + \dfrac{Q}{r} + q \right)^n. \end{cases} \tag{28}$$

By integrating the velocities after each time step, the displacements can be obtained as:

$$u^{n+1} = u^n + \tau^{n+1}\dot{u}^{n+\frac{1}{2}}. \tag{29}$$

Similar equations can be used to compute the other two displacement components, ψ and w. Using the Eqs. (26), (27), and (3)–(13) along with the appropriate boundary conditions and Eqs. (17)–(21) in their finite difference form, the set of equations for the sequential DR algorithm is formed, which is briefly outlined in the following section.

3.1.1. *The DR Algorithm*

a. Set all of the velocity, displacement, stress resultant, and stress couple variables initially to zero, and apply the transverse load q and maximum iteration number N.
b. Set the time increment τ to unity and the number of iterations n to zero.

Table 1. Maximum dimensionless deflection obtained in this article compared to the results obtained by Reddy et al. [16] for a thickness radius ratio of $h/r_o = 0.15$

	Reddy et al. [16]			Present article		
Material constant (n)	Clamped	Simply supported	Roller-supported	Clamped	Simply supported	Roller-supported
0	2.781	10.623	10.623	2.774	10.572	10.572
2	1.515	5.610	5.826	1.511	5.565	5.801
4	1.384	5.217	5.325	1.382	5.200	5.305
8	1.278	4.870	4.909	1.277	4.876	4.850
10	1.250	4.772	4.799	1.251	4.760	4.793
50	1.137	4.348	4.349	1.134	4.346	4.349
100	1.119	4.280	4.280	1.116	4.281	4.281
1000	1.103	4.214	4.214	1.107	4.229	4.229
100,000	1.101	4.207	4.207	1.102	4.217	4.217

c. Compute M and C.
d. Compute the velocities using Eq. (28).
e. Integrate the velocities to achieve the displacements X^n by using Eq. (29).
f. Apply the boundary conditions.
g. Compute the strain components using Eq. (8).
h. Compute the stress resultants using Eq. (11).
i. Check if the right-hand side of Eq. (22) R^n is too small, i.e., $\leq 10^{-6}$ on all interior nodes, stop and print out the static solution X^n, otherwise continue.
j. Calculate $\dot{X}^{n+\frac{1}{2}}$ and c^n.
k. Check if $\sum_j (\dot{X}_j^{n+\frac{1}{2}})^2 \leq 10^{-12}$, stop and print out the static solution X^n, otherwise continue.
l. Set $n = n + 1$, if $n \geq N$ stop, otherwise return to step c and repeat the sequence.

3.2. *Finite Difference Discretization*

To apply the DR method to solve the previously mentioned system of equations, the equations must be discretized. Hence, the central finite difference technique was applied to replace the derivatives. The boundary conditions were imposed via the specification of values at fictitious nodes that are located outside of the plate boundaries. Due to the axisymmetric nature of the loading and the plate geometry, only a radial line of the plate was used, and the governing plate equations were applied to nodal points along this line. Because it is not possible to apply the equations to the center node of the plate, the limiting process suggested by Kobayashi and Turvey [29] was used here to overcome the singularity problem at the center. This scheme was applied to every term with the factor $(1/r)$ in the governing equations, i.e.,

$$\lim_{r\to 0} \frac{u_0}{r} = \frac{du_0}{dr}. \tag{30}$$

3.3. *Verification of the DR Analysis*

To demonstrate the efficiency and accuracy of this numerical study, the results of our analysis for an axisymmetric bending problem of a functionally graded circular plate with clamped, roller-supported, and simply supported boundary conditions were compared to the results of Reddy et al. [16]. The analysis of the FG plate with uniform thickness was conducted for a combination of ceramic and metal. Titanium and zirconia with values of $\nu = 0.288$, $E_c = 151.0$ GPa, and $E_m/E_c = 0.396$ were selected as the constituent materials. A comparison of the numerical results obtained from this study with the analytical results obtained by Reddy et al. [16] is shown in Table 1. For the dimensionless maximum deflection $W_{\max} = 64wD_c/q_o r_o^4$ with $D_c = E_c h^3/12(1-\nu^2)$ and the transverse load $q_o = 0.14$ GPa, good agreement was observed.

4. Results and Discussion

In this article, the axisymmetric bending and stretching of a functionally graded circular and annular plate was numerically studied under combined thermal–mechanical loadings. To achieve this goal, the plate was subjected to a transverse uniform load and a temperature field. An FG plate with uniform and nonuniform thicknesses (Figure 1) under various boundary conditions (simply supported and clamped circular plates as well as clamped-clamped (CC) and clamped-simply supported (CS) in the inner and outer edge of the annular plates was considered. The material properties (which are listed in Table 2) were used from Ref.[2]. Then, a metal/aluminum and ceramic/zirconia system of FGM was considered in which the ceramic-rich top surface was maintained at 300°C, and the metal-rich bottom surface was maintained at 20°C. The stress-free temperature is $T_0 = 0$°C. A mechanical pressure loading of $q = 10$ MPa was also applied to the top surface of the plate in which the ratio of thickness to external radius is $h/r_o = 0.15$. For the annular plate, the ratio of the outer to inner radius was assumed as $r_o/r_i = 5$. The results presented in Table 3 are defined in terms of dimensionless parameters. In this table, the dimensionless radius, thickness, center deflection, stress resultant and moment resultant are expressed as $\bar{r}$, $\bar{z}$, $\bar{w}$, $\bar{N}_r$, and $\bar{M}_r$, respectively.

Figure 2 shows the distribution of the metal volume fraction throughout the thickness of the plate for various values of

Table 2. Material properties of metal, aluminum and ceramic, zirconia in the FGM

Materials	Young's modulus E(GPa)	Poisson's ratio ν	Thermal conductivity coefficient $K(W/mk)$	Thermal expansion coefficient $\alpha(1/^\circ C)$
Aluminum	70	0.3	204	23×10^{-6}
Zirconia	151	0.3	2.09	10×10^{-6}

Table 3. Dimensionless parameters

Parameter	$\bar{r}$	$\bar{w}$	$\bar{z}$	$\bar{N}_r$	$\bar{M}_r$
Definition	r/r_0	w/h	z/h	$N_r r_0^2/E_m h^3$	$M_r r_0^2/E_m h^4$

the grading index n. The temperature distribution throughout the thickness of the FG plate that was calculated from Eq. (6) for various values of n is shown in Figure 3. This figure shows that the temperature change along the thickness of a homogeneous plate consisting completely of metal or ceramic is linear, whereas for an FGM plate, the temperature change is nonlinear. Furthermore, in nonhomogeneous plates, the variation in temperature increases along the thickness with an increase in n such that the temperature of the mid-plane in an FG plate for $n = 10$ is approximately twice of that for $n = 2$. Additionally,

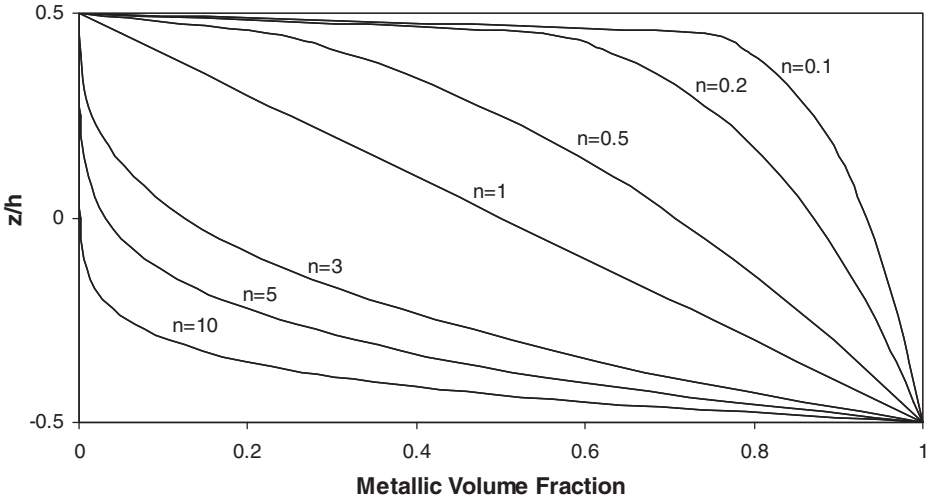

Fig. 2. Variation in the volume fraction of the metallic phase throughout the dimensionless thickness for different values of n.

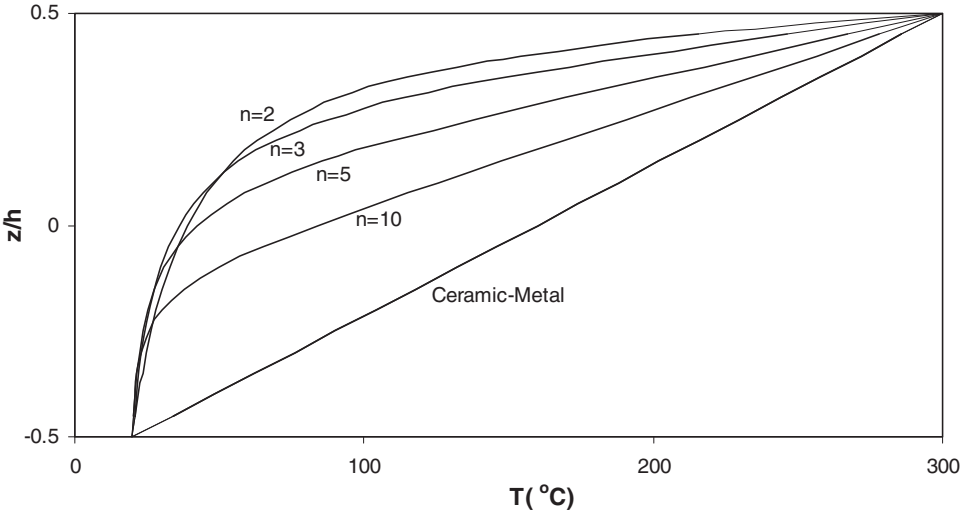

Fig. 3. Temperature distributions throughout the thickness of the FGM plate.

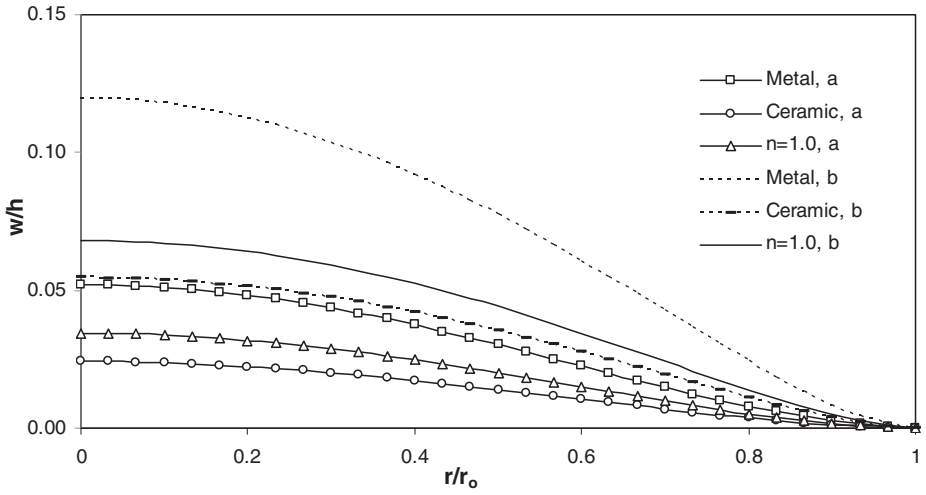

Fig. 4. Dimensionless vertical displacement along the radial direction of the clamped circular FGM plate: (a) uniform thickness and (b) convex thickness profile.

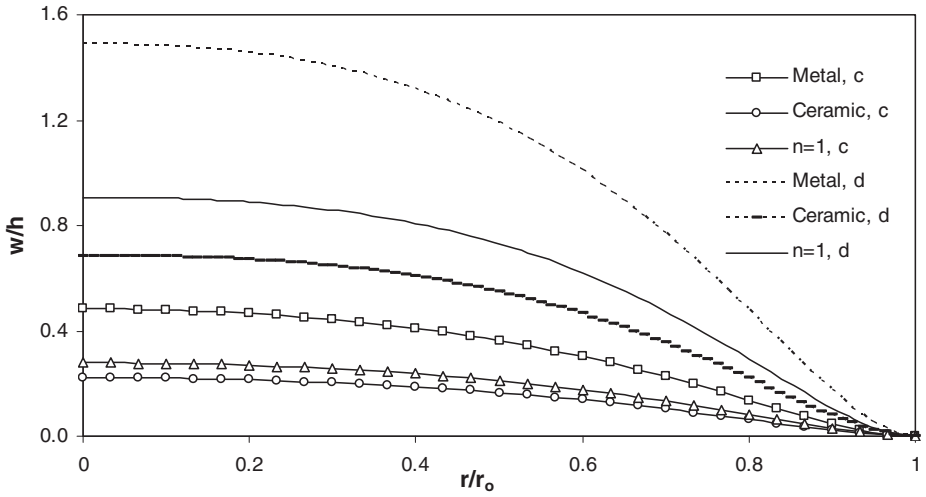

Fig. 5. Dimensionless vertical displacement along the radial direction of the clamped circular FGM plate: (c) linear thickness profile and (d) concave thickness profile.

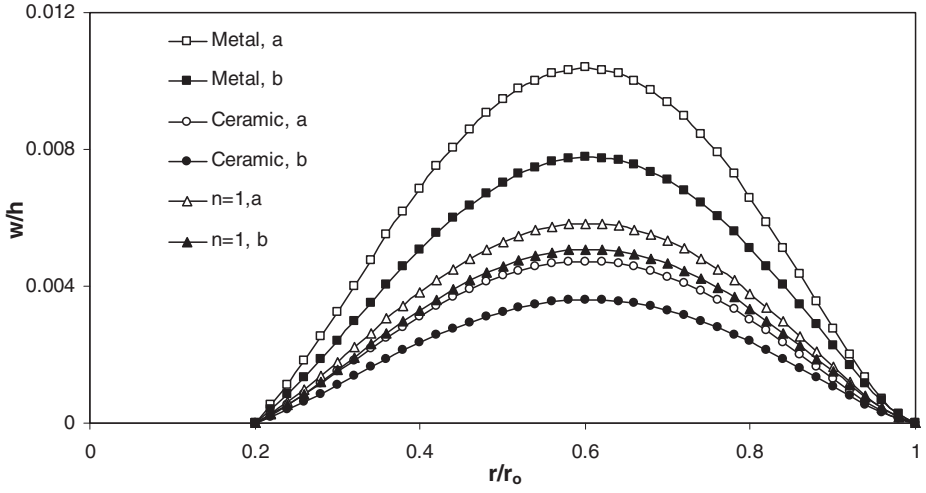

Fig. 6. Comparison of the dimensionless vertical displacement for the convex thickness profile of the CC annular FGM plate under mechanical loading: (a) with thermal loading and (b) without thermal loading.

the temperature in the FG plate is always lower than that in a pure metallic or ceramic plate.

Figures 4 and 5 show the dimensionless vertical displacement $\bar{w}$ along the radial direction of the clamped circular FG plate (for different thickness profiles) that was subjected to mechanical and thermal loading. As expected, due to the stiffness of the plate, the displacement of the concave plate was the largest, and the displacement of a uniform plate was the smallest. For the sake of brevity, the graphs showing the vertical displacement of the simply supported FG plate are omitted. The difference between the ratio of maximum deflection of the plates with nonuniform thicknesses to the uniform plates with homogenous properties is almost 10% greater than that in the FGM plate with $n = 1$. In other words, variation in the thickness has a smaller effect on the deflection of FGM plates compared to homogenous plates.

Figure 6 shows the dimensionless vertical displacement $\bar{w}$ along the radial direction of the CC annular FG plate subjected to mechanical loading with and without thermal gradients in the plates with convex thickness profiles. The

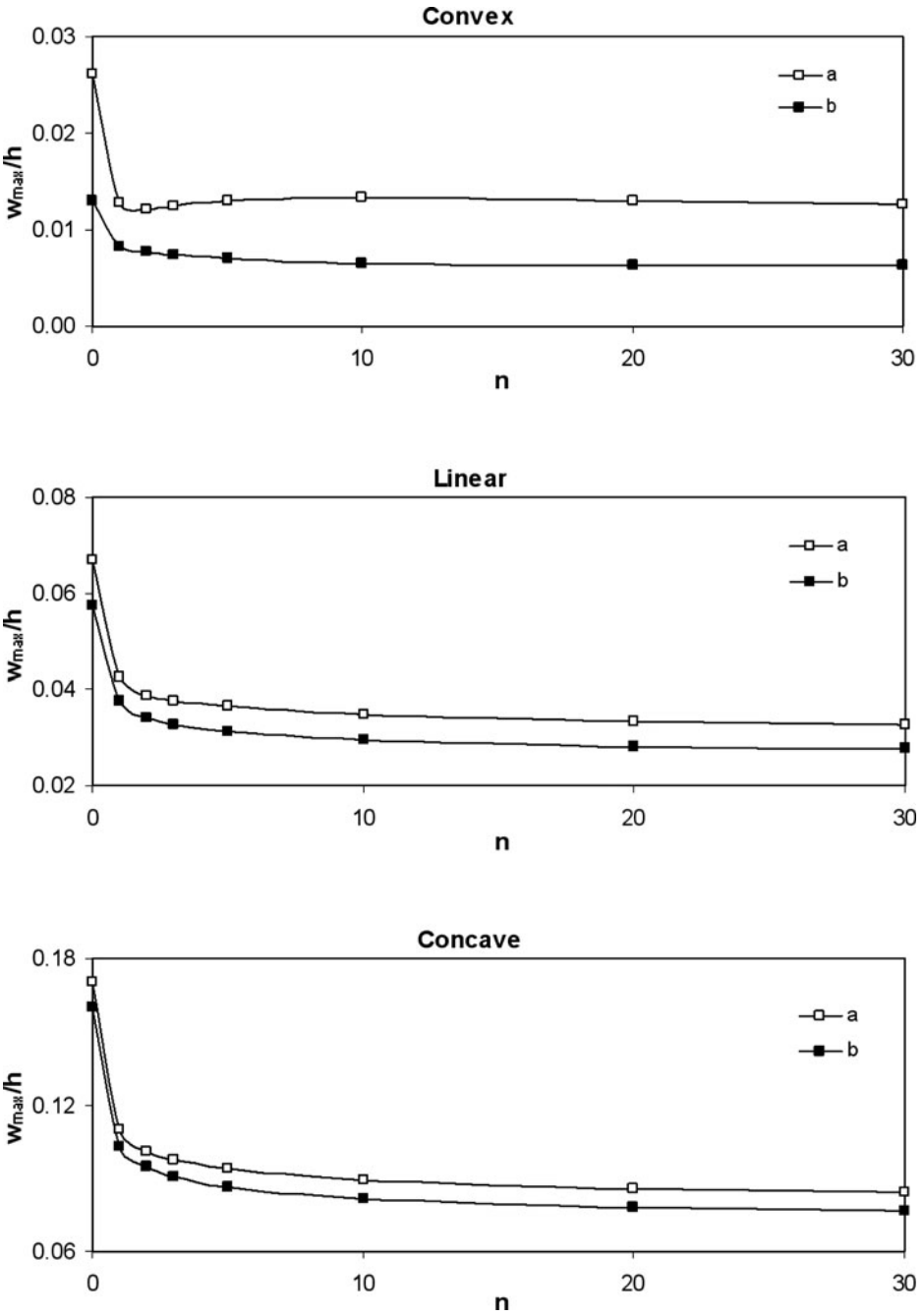

Fig. 7. Variation in the dimensionless vertical displacement with different volume fractions, n, for convex, linear, and concave thickness profiles of the CS annular FGM plate under mechanical loading: (a) with thermal loading and (b) without thermal loading.

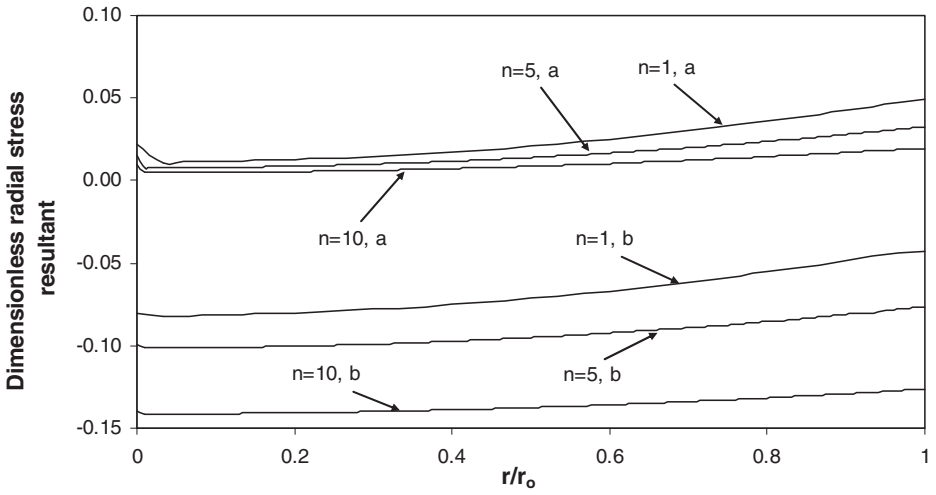

Fig. 8. Dimensionless stress resultant of the simply supported circular FGM plate with uniform thickness under mechanical loading: (a) without thermal loading and (b) with thermal loading.

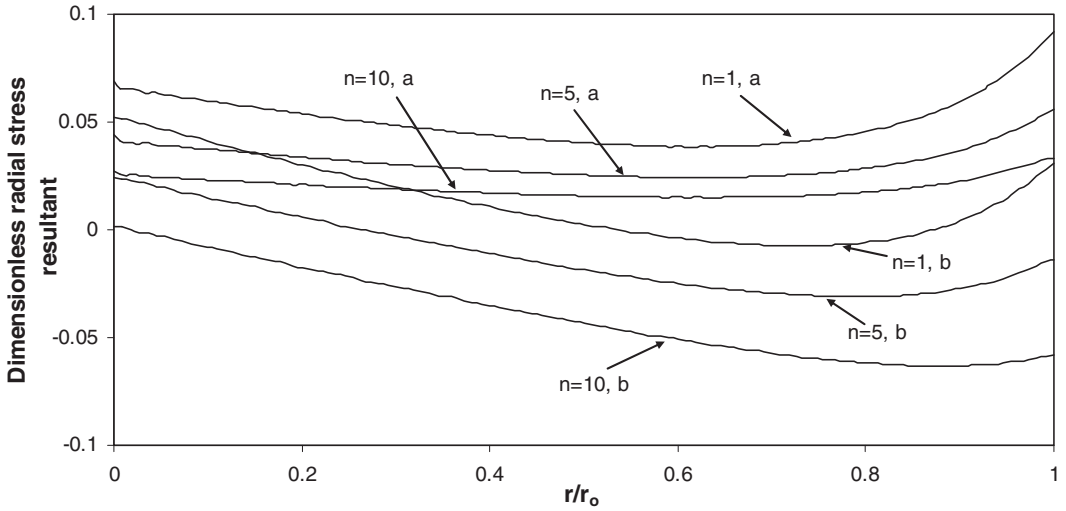

Fig. 9. Dimensionless radial stress resultant of the simply supported circular FGM plate with linear thickness under mechanical loading: (a) without thermal loading and (b) with thermal loading.

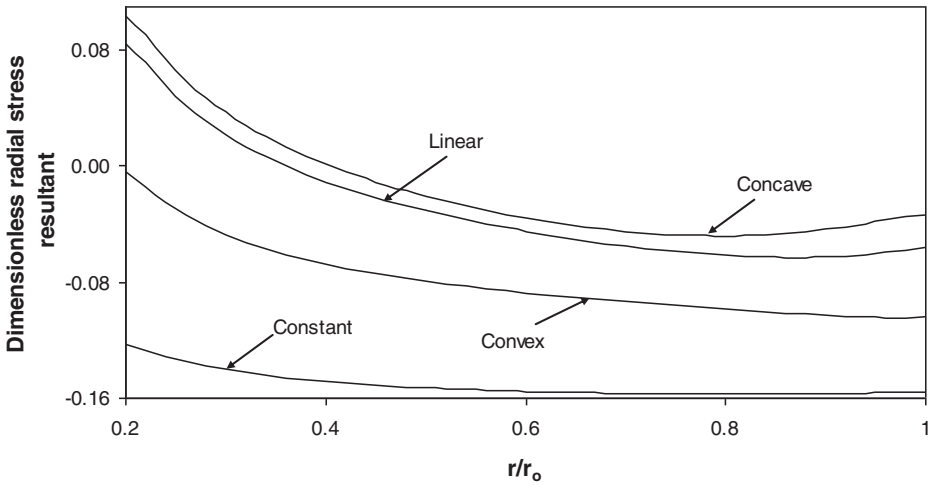

Fig. 10. Dimensionless radial stress resultant of the CS annular FGM plate.

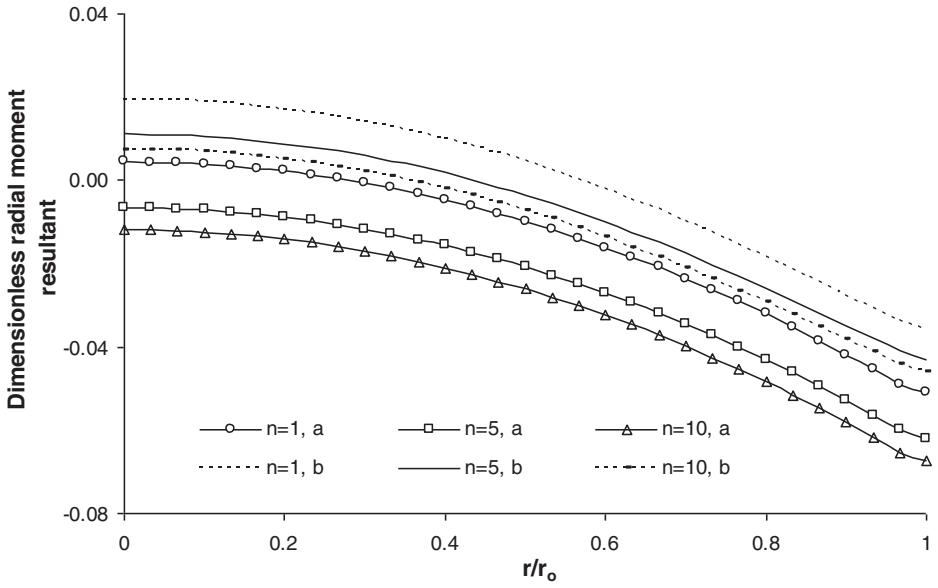

Fig. 11. Dimensionless moment resultant along the radial direction of the clamped circular FGM plate: (a) uniform thickness and (b) convex thickness profile.

temperature causes a larger increase in the maximum deflection in the metallic or ceramic plate instead of the nonhomogeneous FGM plate. For example, the maximum deflection of an FGM plate with $n = 1$ with the temperature field is about 15% greater than that of the plate without the temperature field. However, the difference is about 35% for the homogeneous (metallic or ceramic) plate.

The maximum dimensionless deflection of the CC annular FG plate with convex, linear, and concave thickness profiles with respect to different volume fractions, n, that was subjected to mechanical loading with and without the temperature field is shown in Figure 7. The largest and smallest differences between the maximum deflections with and without the temperature field are related to the convex and concave plates, respectively, which can be attributed to different values of the mechanical and thermal strains due to the different thickness profiles of the plates. As previously mentioned, the smallest difference of maximum deflection of the plate with and without thermal gradients occurred in a FG plate with $n = 1$ for all of the thickness profiles. The amount of maximum deflections in the presence of thermal loading increased by about 54, 13.6, and 6.8% for the metal, ceramic, and FGM plates, respectively, compared to the case without the thermal gradient.

The dimensionless stress resultant, $\bar{N}_r$, for the simply-supported circular FG plate with two different thickness profiles (uniform and linear) is shown in Figures 8 and 9. As n increases, the material properties of the plate become similar to

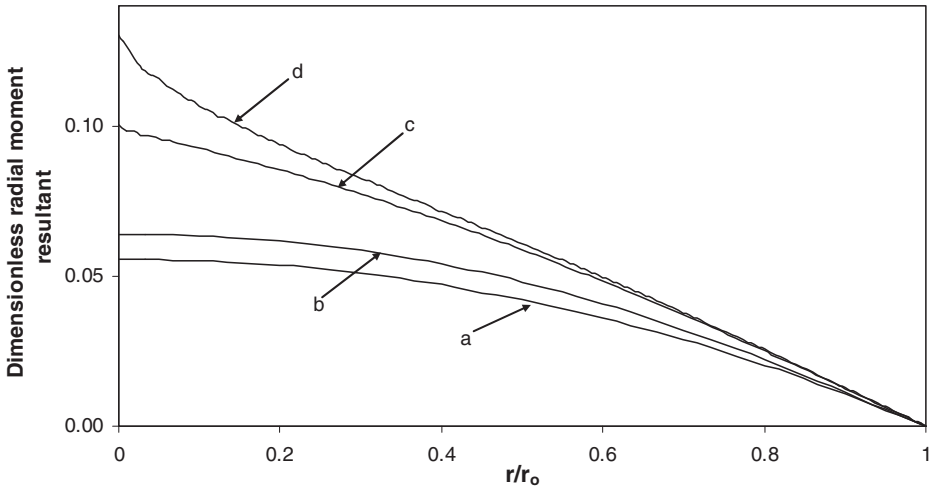

Fig. 12. Comparison between the dimensionless moment resultant for the simply supported FGM plate ($n = 1$) with different thickness profiles: (a) uniform, (b) convex, (c) linear, and (d) concave.

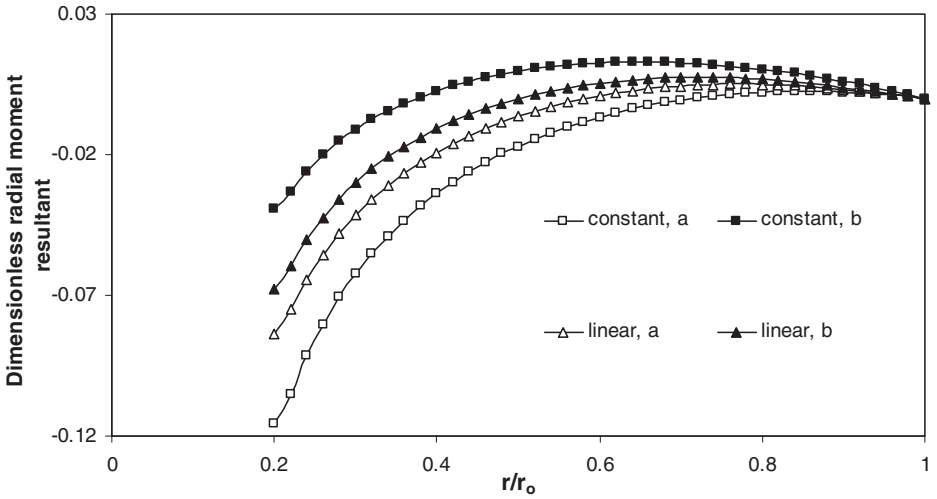

Fig. 13. Distribution of the dimensionless resultant moment along the radial direction for two thickness profiles of the clamped-simply supported annular FGM plate: (a) with thermal loading and (b) without thermal loading.

those of ceramic. Therefore, an increase in the stiffness causes a decrease in the strain value and, consequently, a decrease in the radial stress resultant for a given radius. Furthermore, unlike the variable thickness plate, a variation in stiffness (and consequently $\bar{N}_r$) is not significant along the radial direction for uniform thickness profiles.

On the other hand, the difference between the values of $\bar{N}_r$ along the radius for different material constants, n, increased due to the applied thermal load. For example, the difference between the materials for $n = 1$ and $n = 10$ was approximately 40% at the center of the plate with uniform thickness. Generally, for both of the plates with uniform and linear thicknesses, the application of the temperature field reduced the amount of $\bar{N}_r$ along the radial direction.

The variation of $\bar{N}_r$ in the radial direction in the plates with linear thickness was significantly greater than that of the plates with uniform thickness, which is related to the thickness variation of the plate, as shown in Figure 9. Furthermore, the amount of $\bar{N}_r$ increased in the nonuniform plates for a given radius due to an increase in the mechanical strain and the stress compared to the uniform plates. The application of the thermal gradient to the plate with a linear thickness profile causes less compressive stresses along the thickness, which is a result of the larger amount of mechanical strain compared to thermal strain in this thickness profile.

Figure 10 shows the variation of $\bar{N}_r$ along the radius for various thickness profiles (constant, convex, linear, and concave) in clamped-simply supported annular FGM plates with $n = 1$. If the temperature field is applied to a plate that is subject to a uniform mechanical load of $q = 10$ MPa, then $\bar{N}_r$ becomes compressive for uniform and convex plates, whereas $\bar{N}_r$ exhibits higher values for linear and concave plates and becomes tensile from the center to $r/r_o = 0.4$. Furthermore, the highest and lowest variations of $\bar{N}_r$ occurred in the plates with a concave and constant thickness along their radius, respectively, which was caused by different stiffness variations that modify the mechanical and thermal strains.

Figure 11 shows the dimensionless resultant moment $\bar{M}_r$ along the radial direction. As the material constant n increases, $\bar{M}_r$ decreases. As previously mentioned, the stiffness of the plate increases due to an increase in the material constant n if the material property tends to be ceramic with a higher stiffness.

Figure 12 shows the distribution of the dimensionless resultant moment $\bar{M}_r$ along the radial direction for different thickness profiles. $\bar{M}_r$ attains a minimum value for the uniform plate and a maximum value for the concave thickness profile. For example, the value of $\bar{M}_r$ for the concave plate is 2.3 times greater than that of the uniform plate at the center. This indicates that the concave plate has higher strain values due to the reduction of stiffness along its radius. Furthermore, because of the higher reduction rate of thickness along the radial direction in the concave plate, the stiffness and $\bar{M}_r$ in the radial direction decrease significantly compared to the plate with uniform thickness.

Figure 13 shows the distribution of the dimensionless resultant moment $\bar{M}_r$ along the radial direction in the CS annular FG plate with the consideration of the thermal effects. In the presence of thermal loading, $\bar{M}_r$ decreases compared to the case with purely mechanical loading. Also, the difference between $\bar{M}_r$ with and without thermal loading in the plate with constant thickness is much greater than the plate with variable thickness. For example, the difference of $\bar{M}_r$ in the inner edge of the annular FG plate with a constant thickness profile is 2.5 times greater than the difference in the plate with a linear thickness profile. The reasons for these variations are similar to the previously mentioned reasons for $\bar{N}_r$.

5. Conclusions

The axisymmetric bending and stretching of a functionally graded circular plate with variable thickness under thermal and uniform transverse mechanical loading was considered.

Based on the FSDT, new equilibrium equations were developed, and a dynamic relaxation method along with a finite difference discretization technique was used to solve these equations. The effects of the material constant n, boundary conditions, and different thickness profiles are studied along with combined thermal-mechanical loading. Some general conclusions are listed as follows:

- Variation in the thickness has a smaller effect on the deflection of the FGM plates compared to the homogenous plates.
- For the annular FG plates with clamped-clamped boundary conditions subjected to mechanical loading, the difference between the maximum deflections with and without thermal loading is minimal for the FGM plate with $n = 1$.
- For plates with variable thicknesses, the difference between the maximum deflections with or without temperature field is largest for the convex plate and smallest for the concave plate.
- An increase in the thickness profile variation in the plates resulted in a greater variation in $\bar{N}_r$ along the radius; $\bar{N}_r$ had the largest amount of variation for the concave plate and smallest amount of variation for the plate with constant thickness along the radius.
- The application of the thermal gradient to the plate with a variable thickness profile causes the stress to be less compressive along the thickness.
- For all of the thickness profiles, as the material constant n increases, $\bar{N}_r$ and $\bar{M}_r$ decrease.
- The difference between $\bar{M}_r$ with and without thermal loading is significantly greater in the plate with constant thickness rather than the plate with variable thickness.

References

[1] M. Koizumi, The concept of FGM ceramic transactions, Funct. Graded Mater., vol. 34, no. 1, pp. 3–10, 1993.

[2] G.N. Praveen and J.N. Reddy, Nonlinear transient thermoelastic analysis of functionally graded ceramic-metal plates, Int. J. Solids Struct., vol. 35, pp. 4457–4476, 1998.

[3] J.N. Reddy and C.D. Chin, Thermoelastical analysis of functionally graded cylinders and plates, J. Therm. Stresses, vol. 21, pp. 593–626, 1998.

[4] A.J.M. Ferreira, C.M.C. Roque, R.M.N. Jorge, G.E. Fasshauer, and R.C. Batra, Analysis of functionally graded plates by a robust meshless method, Mech. Adv. Mater. Struct., vol. 14, pp. 577–587, 2007.

[5] Y. Ootao and Y. Tanigawa, Three-dimensional transient thermal stresses of functionally graded rectangular plate due to partial heating, J. Therm. Stresses, vol. 22, pp. 35–55, 1999.

[6] J.N. Reddy and C.D. Cheng, Three-dimensional thermo-mechanical deformations of functionally graded rectangular plates, Euro. J. Mech. A/Solids, vol. 20, pp. 841–855, 2001.

[7] G.N. Praveen, C.D. Chin, and J.N. Reddy, Thermoelastic analysis of functionally graded ceramic–metal cylinder, ASCE J. Eng. Mech., vol. 125, pp. 1259–1267, 1999.

[8] Y. Obata and N. Noda, Steady thermal stresses in a hollow circular cylinder and a hollow sphere of a functionally gradient material, J. Therm. Stresses, vol. 17, pp. 471–488, 1994.

[9] L.S. Ma and T.J. Wang, Nonlinear bending and postbuckling of functionally graded circular plates under mechanical and thermal loadings, Int. J. Solids Struct., vol. 40, pp. 3311–3330, 2003.

[10] M. Bayat, B.B. Sahari, M. Saleem, A. Aidy, and S.V. Wong, Thermoelastic solution of a functionally graded variable thickness rotating disk with bending based on the first-order shear deformation theory, Thin-Walled Struct., vol. 47, pp. 568–582, 2009.

[11] M. Bakhshi, A. Bagri, and M.R. Eslami, Coupled thermoelasticity of functionally graded disk, Mech. Adv. Mater. Struct., vol. 13, pp. 219–225, 2006.

[12] M. Ohga and T. Shigematsu, Bending analysis of plates with variable thickness by boundary element-transfer matrix method, Comput. Struct., vol. 28, pp. 635–641, 1988.

[13] D.G. Fertis and M.M. Mijatov, Equivalent systems for variable thickness plates, ASCE J. Eng. Mech., vol. 115, pp. 2287–2300, 1989.

[14] A.M. Zenkour, An exact solution for the bending of thin rectangular plates with uniform, linear, and quadratic thickness variations, Int. J. Mech. Sci., vol. 45, pp. 295–315, 2003.

[15] Y. Xu and D. Zhou, Three-dimensional elasticity solution of functionally graded rectangular plates with variable thickness, Compos. Struct., vol. 91, pp. 56–65, 2009.

[16] J.N. Reddy, C.M. Wang, and S. Kitipornchai, Axisymmetric bending of functionally graded circular and annular plates, Euro. J. Mech. A/Solids, vol. 18, pp. 185–199, 1999.

[17] J.N. Reddy, Mechanics of Laminated Composite Plates: Theory and Analysis, CRC Press, New York, 1997.

[18] S.P. Timoshenko and S. Woinowsky-Krieger, Theory of Plates and Shells, McGraw-Hill, New York, 1970.

[19] A.S. Day, An introduction to dynamic relaxation, The Engineer, vol. 219, pp. 218–221, 1965.

[20] G.J. Turvey and G.T. Lim, A parametric study of the axisymmetric full-range response of thickness-tapered circular steel plates, Comput. Struct., vol. 22, pp. 459–468, 1986.

[21] M.E. Golmakani and M. Kadkhodayan, Nonlinear bending analysis of annular FGM plates using higher-order shear deformation plate theories, Compos. Struct. DOI: 10.1016/j.compstruct.2010.06.024.

[22] M. Kadkhodayan, J. Alamatian, and G.J. Turvey, A new fictitious time for the dynamic relaxation (DXDR) method, Int. J. Numer. Meth. Eng., vol. 74, pp. 996–1018, 2008.

[23] M. Rezaiee-Pajand and J. Alamatian, Nonlinear dynamic analysis by dynamic relaxation method, J. Struct. Eng. Mech., vol. 28, pp. 549–570, 2008.

[24] M. Kadkhodayan and L.C. Zhang, A consistent DXDR method for elastic–plastic problems, Int. J. Numer. Meth. Eng., vol. 38, pp. 2413–2431, 1995.

[25] M. Salehi and H. Aghaei, Dynamic relaxation large deflection analysis of non-axisymmetric circular viscoelastic plates, Comput. Struct., vol. 83, pp. 1878–1890, 2005.

[26] M. Kadkhodayan, L.C. Zhang, and R. Sowerby, Analysis of wrinkling and buckling of elastic plates by DXDR method, Comput. Struct., vol. 65, pp. 561–574, 1997.

[27] M. Kadkhodayan and L.C. Zhang, A simple algorithm for stamping circular plates by hemispherical punches, J. Mater. Proc. Technol., vol. 68, pp. 33–38, 1997.

[28] L.C. Zhang and T.X. Yu, Modified adaptive dynamic relaxation method and application to elastic-plastic bending and wrinkling of circular plate, Comput. Struct., vol. 33, pp. 609–614, 1989.

[29] H. Kobayashi and G.J. Turvey, On the application of a limiting process to the dynamic relaxation analysis of circular membranes, circular plates and spherical shells, Comput. Struct., vol. 48, no. 6, pp. 1107–1116, 1993.